34th Annual International Conference of the IEEE EMBS
San Diego, California USA, 28 August - 1 September, 2012

Automatic Measurements of Choroidal Thickness in EDI-OCT Images

Jing Tian, Pina Marziliano, IEEE Member, Mani Baskaran, Tin Aung Tun and Tin Aung

***Abstract*— Enhanced Depth Imaging (EDI) optical coherence tomography (OCT) provides high-definition cross-sectional images of the choroid *in vivo*, and hence is used in many clinical studies. However, measurement of choroidal thickness depends on the manual labeling, which is tedious and subjective of inter-observer differences.**

In this paper, we propose a fast and accurate algorithm that could measure the choroidal thickness automatically. The lower boundary of the choroid is detected by searching the biggest gradient value above the retinal pigment epithelium (RPE) and the upper boundary is formed by finding the shortest path of the graph formed by valley pixels using dynamic programming. The average of Dice's Coefficient on 10 EDI-OCT images is 94.3%, which shows good consistency of the algorithm with the manual labeling. The processing time for each image is about 2 seconds.

I. Introduction

The choroid (lying between the retina and the sclera as shown in Fig. 1), is the vascular layer providing the metabolic support to the retinal pigment epithelium (RPE), supplying blood to the optic nerve and absorbing the excess light penetrating the retina [1]. The quantitative and qualitative evaluation of the choroid thickness is important in order to reveal its relationship with the retinal diseases and glaucoma. Quigley et al. proposed that a mere 50 micrometer choroid expansion in angle closure glaucoma patients can increase the intraocular pressure to harmful levels [2]. There has also been an increasing interest in investigating its correlation with the age, gender, axial length and intra-ocular pressure in healthy human eyes [3].

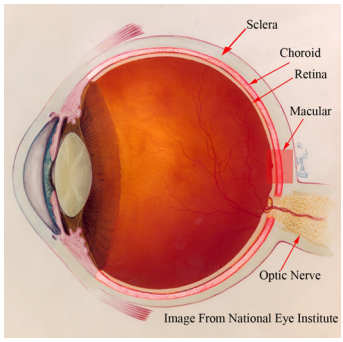

Fig. 1. Anatomy of the human eye: the choroid is the vascular layer between the sclera and the retina.

Therefore, the research on measuring the choroidal thickness *in vivo* has attracted the attention of many clinicians and scientists. Traditionally, histological evaluation is used but the measurement is not accurate as the structures of the choroid are destroyed when taking the tissue samples. High frequency ultrasonography has also been used to measure the choroidal thickness in the eyes of chicken but the high energy dispersion makes it unsuitable for imaging the human eyes [4]. Optical coherence tomography (OCT), an emerging non-contact, non-invasive and high resolution imaging modality, could provide the *in vivo* cross-sectional image of the human retina [5]. However, the absorption by the RPE and the scattering by dense vascular structure limit the ability of the conventional OCT to image the choroid accurately [6] . In 2008, Spaide et al. proposed the Enhanced Depth Imaging OCT (EDI-OCT) system, to improve the visualization of the choroid [7]. Essentially, EDI-OCT system places the objective lens of the Spectral-Domain OCT closer to eye, so the light backscattered from the choroid is closer to the zero delay line and hence the sensitivity is enhanced.

In several recent studies, the choroidal thickness is measured using EDI-OCT to study its relationship with the retinal diseases [8] and to monitor patients after treatment [9]. Experiments have been also conducted in healthy eyes of Japanese population [1], [10]. However, the choroidal thickness measurements are based on the manual labelings of the boundaries which is tedious and time-consuming, especially when the population of study is large. Furthermore, the measurements lack objectivity and are prone to inter-observer errors. For EDI-OCT to become a clinically practical tool for determining choroidal thickness, an automatic and accurate measurement algorithm must be developed.

There has been a number of researches conducted to segment the retinal layer in OCT images [11], [12], [13], but they rely on uniform layer structure and well-defined boundaries in retina and do not perform well for the choroid segmentation. The difficulties of choroid segmentation are highlighted as follows:

1) The contrast between the choroid and sclera in OCT images is low, i.e. the histograms of choroid and sclera region are not separable, which makes the intensity based thresholding and classification useless;
2) Due to the presence of the vascular structure, the intensity of the choroid is inhomogeneous and the texture of the choroid is inconsistent;
3) The interface between the sclera and choroid is often very weak as compared to retinal layers and even invisible in some locations.

Veteran et al. [14] have devised a two stage statistical model to automatically detect the choroid boundaries in the 1060-nm OCT images of both healthy eyes and pathological eyes.

J.Tian and P. Marziliano are with the School of Electrical and Electronic Engineering, Nanyang Technological University, Singapore. Email: ti0001ng, epina@ntu.edu.sg

Mani Baskaran, Tin Aung Tun and Tin Aung are with the Singapore Eye Research Institute, Singapore.

However, the model requires extensive training and takes about 30 seconds to process each image. The mean error is 13%. Up to our knowledge, it is the only automatic algorithm to evaluate the choroidal thickness.

In this paper, we present an automatic algorithm that could measure the choroidal thickness accurately and significantly reduce the processing time. The lower boundary of the choroid is detected by searching the biggest gradient value above the RPE and the upper boundary is formed by finding the shortest path of the graph formed by valley pixels (local minimums of A-scan) using dynamic programming. The details of the algorithm are presented in Section II and the experiments and the results are presented in Section III. The conclusion and the future work are discussed in Section IV.

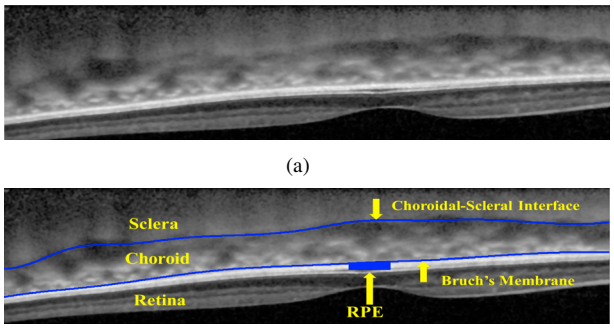

(a)

(b)

Fig. 2. (a) EDI-OCT image in the macular region of the human eye. (b) The Bruch's Membrane and the choroidal-scleral interface are manually labeled by the ophthalmologists.

II. Method

The EDI-OCT provides the high-contrast cross-sectional image of the choroid *in vivo* as shown in Fig. 2 (a) (an inverted image of retina and choroid is given here as captured and analysed in this study). The choroid is bounded by two structural interfaces, choroidal-scleral interface (denoted as C_{csi}) and Bruch's Membrane (denoted as C_{bm}), which are labeled by the ophthalmologists as shown in Fig. 2 (b) and the distance in between is the choroidal thickness.

This section describes an automatic algorithm that could detect the C_{csi} and C_{bm} from the EDI-OCT images and the schematic overview is shown in Fig. 3. The details of the algorithm are presented in Section II-A to Section II-C.

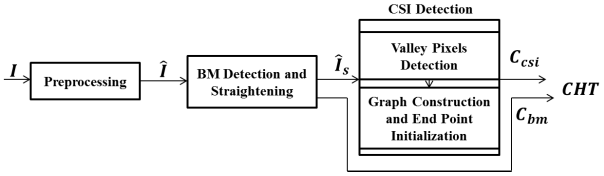

Fig. 3. The overview of the automatic measurements of choroidal thickness algorithm.

A. Preprocessing

To suppress additive thermal noise and electronic noise, the original EDI-OCT image denoted as $I(x, y)$ for $(x, y) \in [1, N_c] \times [1, N_r]$ is first convolved with a 5×5 Wiener filter, which is adaptive to the estimated noise level. Then each point in the A-scan is replaced by an N-point moving average to reduce the spurious peaks caused by the speckle noise. The larger value of N will reduce the number of spurious peaks with the risk of wrong delineation of CSI. In our algorithm, N can be set to $\{5, 6 \ldots 10\}$. Denote the image after denoising as $\hat{I}(x, y)$.

B. BM Detection and Straightening

It is observed that the RPE layer is the brightest layers within the EDI-OCT image, so the pixels with the highest intensities in the A-scans is assigned as the ridge of RPE, which is denoted as C_{rp} and calculated in Eq. (1)

$$C_{rp} = \{(x, y_{rp}) | x \in [1, N_c], y_{rp} = \arg\max_{u \in [1, N_r]} \hat{I}(x, u)\}. \quad (1)$$

Bruch's membrane is the upper boundary of the RPE and can be located by searching for the pixels with the biggest gradient value above the C_{rp} as defined by Eq. (2)

$$bm = \{(x, y_{bm}) | x \in [1, N_c], y_{bm} = \arg\max_{u \in [y_{rp} - \Delta, y_{rp}]} \boldsymbol{g} \cdot \hat{I}(x, u)\}, \quad (2)$$

where $\boldsymbol{g}$ is the gradient operator $\boldsymbol{g} = [-1 \ -1 \ -1 \ 0 \ 1 \ 1 \ 1]$ and Δ is the search range. Basically, the gradient operator $\boldsymbol{g}$ computes the difference between sum of neighbouring pixels below and above the pixel (x, u) and the value is maximized at the Bruch's membrane location if we assume the intensities of pixels in the RPE layer is greater than the ones in the choroid. In order to form the smooth boundary, a 4th order polynomial $f_{bm}(x) = p_4 x^4 + p_3 x^3 + p_2 x^2 + p_1 x + p_0$ is used to fit the points in bm and the Bruch's membrane is denoted as $C_{bm} = \{(x, f_{bm}(x))\}$, where

$$(p_4, p_3, p_2, p_1, p_0) = \arg\min \sum_{x=1}^{N_c} (y_{bm} - f_{bm}(x))^2.$$

The result of the Bruch's membrane detection is illustrated in Fig. 4 (b).

Each A-scan of the OCT image is shifted up or down so that the Bruch's membrane is straight in the new image $\hat{I}_s(x, y)$ to avoid inaccurate shortcuts across the choroid due to the natural retinal curvature in EDI-OCT image when detecting the choroidal-scleral interface using graph search. The results of the straightened image is shown in Fig. 4 (c).

C. CSI Detection

Because a discontinuity of the refractive index creates a distinct valley in the OCT A-scan according to the OCT fundamental principle, the choroidal-scleral interface corresponds to a smooth curve formed by valley pixels, which are detected as described in Section II-C.1.

However, the valley pixels are also caused by the speckle noise and the blood vessels in the choroid as shown in Fig. 5. It is assumed that the choroidal-scleral interface does not have abrupt transitions between the adjacent A-scans, so the valley pixels caused by the choroidal-scleral interface

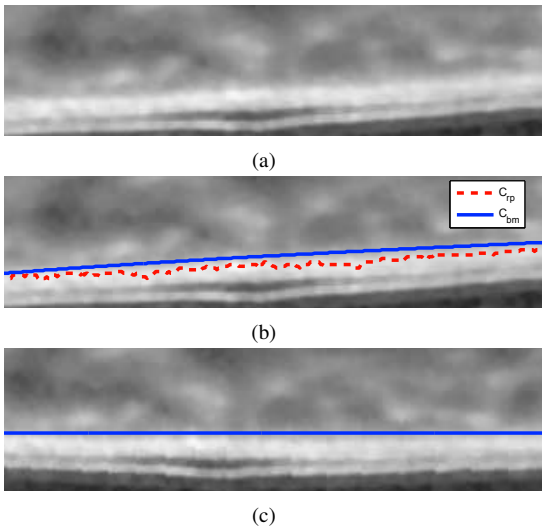

Fig. 4. BM detection algorithm. (a) Part of the EDI-OCT image, (b) The detected RPE and Bruch's membrane. (c) The new image $\hat{I}_s$ has the flat Bruch's membrane.

are close to each other and can be connected to form a smooth contour. On the other hand, the valleys caused by the speckle noise and blood vessels in the choroid region appears randomly located as illustrated in Fig. 5.

Hence, a graph search method is used to distinguish the valley pixels caused by the real boundary from the others. We represent every valley pixel as a vertex of a directed graph $\boldsymbol{G}$ and each vertex is connected to the vertices in the adjacent columns. The choroidal-scleral interface corresponds to the shortest path between the vertices in both ends. The construction of the graph and the end point initialization are presented as follows.

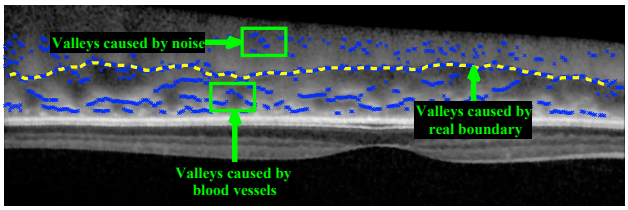

Fig. 5. The valleys (local minimums) of the A-scans are used as the feature to detect the choroidal-scleral interface. However, there are also valleys caused by the speckle noise and the blood vessels in the choroid region.

1) Valley Pixels Detection: All the valley pixels are detected column by column as defined in Eq. (3)

$$AllValleys = \{(x,y)|x \in [1, N_c], y \in \text{ValleyDet}(g^x, \delta)\}, \tag{3}$$

where ValleyDet is the algorithm to detect local minimums in each A-scan as defined in Algorithm 1, g^x is the intensities of the pixels in column x of $\hat{I}_s$, $g^x(y) = \hat{I}_s(x,y)$, and δ is the variation threshold (the variations less than δ is ignored).

2) Graph Construction and End Point Initialization: To construct graph $\boldsymbol{G} = (\boldsymbol{V}, \boldsymbol{E})$, each valley pixel is assigned as a vertex of $\boldsymbol{G}$, $AllValleys \subset \boldsymbol{V}$. Every vertex is connected to the vertices in the adjacent $N_{neighbour}$ column as defined

Algorithm 1 $\boldsymbol{V} = \text{ValleyDet}(g, \delta)$

$L_{max} = 1$; $u_{max} = 1$; $u_{min} = 1$
for $u = 2 : N_r$
  if $g(u) > g(u_{max})$, then $u_{max} = u$ end
  if $g(u) < g(u_{min})$, then $u_{min} = u$ end
  if L_{max}
    if $g(u) < g(u_{max}) - \delta$,
      then $u_{min} = u$, $L_{max} = 0$ end
  else
    if $g(u) > g(u_{min}) + \delta$,
      then $u_{min} \in \boldsymbol{V}$, $u_{max} = u$, $L_{max} = 1$ end
  end
end

in Eq. (4).

$$\boldsymbol{E} = \{(\boldsymbol{a}, \boldsymbol{b})|x_b - x_a \in [1, N_{neighbour}]\}, \tag{4}$$

where $\boldsymbol{b}$ is a vertex in the next ($[1, N_{neighbour}]$) column of vertex $\boldsymbol{a}$, and $(\boldsymbol{a}, \boldsymbol{b})$ represents an edge starting from $\boldsymbol{a}$ and ending with $\boldsymbol{b}$. The weight of each edge is assigned according to Eq. (5)

$$w_{\boldsymbol{ab}} = \begin{cases} ||\boldsymbol{a} - \boldsymbol{b}||^2, & \text{if } |y_a - y_b| < T_y \\ w_{max}, & \text{otherwise.} \end{cases} \tag{5}$$

The parameter T_y is the maximum allowed difference of choroidal-scleral axial location between adjacent columns and w_{max} is a very large number that penalize the path having sudden transition (illustrated as $(\boldsymbol{v_{11}}, \boldsymbol{v_{21}})$ in Fig. 6 (a)). When there are no valleys located within the distance $[0, T_y]$ in the next column, the valleys in the next $N_{neighbour}$ columns would be chosen and added to the path (illustrated as $(\boldsymbol{v_{22}}, \boldsymbol{v_{34}})$ in Fig. 6 (a)). The parameter $N_{neighbour}$ controls the smoothness of the shortest path.

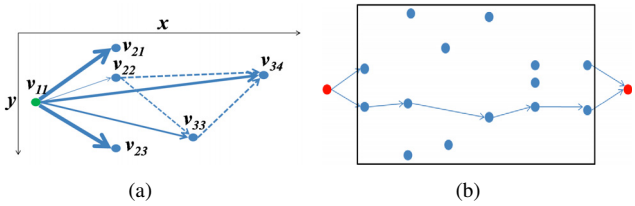

Fig. 6. (a) Construction of graph $\boldsymbol{G}$, each valley pixel is a vertex of the graph and is connected to the vertex in the adjacent column; (b) Automatic end point initialization.

When there are more than one vertex in the first and last columns, finding the shortest path requires the selection of starting and ending points. Here we use the automatic end point initialization method as proposed in [11] to avoid the manual selection process as demonstrated in Fig. 6(b). Two vertices are added to both ends of the graph and are connected to the neighbouring $N_{neighbour}$ with the minmum edge weight 0.01. The shortest path between the two newly added vertices are considered as the estimated location of the choroidal-scleral interface, which can be found by using Dijkstra algorithm. The vertices on the shortest path are transformed from the straightend image to the original image and then fitted with a B-form least square cubic spline to

generate the final boundary C_{csi}. The segmented choroid is the area between C_{bm} and C_{csi} as defined in Eq. (6)

$$CHT = \{(x, y)|x \in [1, N_c], y \in [y_{csi}, y_{bm}]\}, \quad (6)$$

where $(x, y_{csi}) \in C_{csi}, (x, y_{bm}) \in C_{bm}$.

III. Experiments and Results

Our algorithm is tested on ten images captured using EDI-OCT on the SPECTRALIS® system at the Singapore Eye Research Institute. The images are labeled as $f_n, n = 1, 2 \ldots 10$ and each image is $N_r \times N_c = 496 \times 1530\ pixels^2$ and the scan dimension is $1.9 \times 9.1mm^2$, therefore the axial and lateral resolutions are $3.83\mu m/pixel$ and $4.95\mu m/pixel$ respectively. The algorithm is implemented in Matlab R2008a using an Intel Core 2 Quad CPU Q9400 @$2.66GHz$ and $2.67GHz$ computer. The parameters of the algorithm $(N, \Delta, \delta, N_{neighbour}, T_y, w_{max})$ are set to $(5, 20, 3, 8, 5, 100)$ for all the experiments. The results from the algorithm are compared with the ground truth, which is the average of manual labelings from two ophthalmologists.

In the manual labeling experiments, the positions of the Bruch's membrane at discrete locations (5 to 10 locations) are indicated by the observer $i \in \{1, 2\}$. A cubic spline is used to generate the whole curve C^i_{bm} and the average of C^1_{bm} and C^2_{bm} is considered as the ground truth C^0_{bm}. The same process is repeated to get C^0_{csi}. The manual labeled choroid region CHT^0 is the area between C^0_{bm} and C^0_{csi}. Dice's Coefficient is used to evaluate the segmentation result of the algorithm as defined in

$$\text{Dice}_{CHT} = \frac{2|CHT \cap CHT^0|}{|CHT| + |CHT^0|}.$$

The mean of the Dice_{CHT} on 10 images is 94.3% with the maximum up to 98.93% and the minimum of 86.1%. The results of the best case, median case and worst cases are demonstrated in Fig. 7. The overall thickness measurements are consistent. Our detection results follow the valley pixels more closely while the manual labelings are smoother. The reason for the relative large error is due to the small CHT area in the last image. The mean processing time for each image is about 2 seconds.

IV. Conclusion and Future Work

In conclusion, a fast and accurate algorithm that could measure the choroid thickness using EDI-OCT images has been developed. The measurement results of the 10 images are consistent with the manual labelings of the ophthalmologists. As a future work, we would like to use the proposed algorithm to conduct more clinical studies.

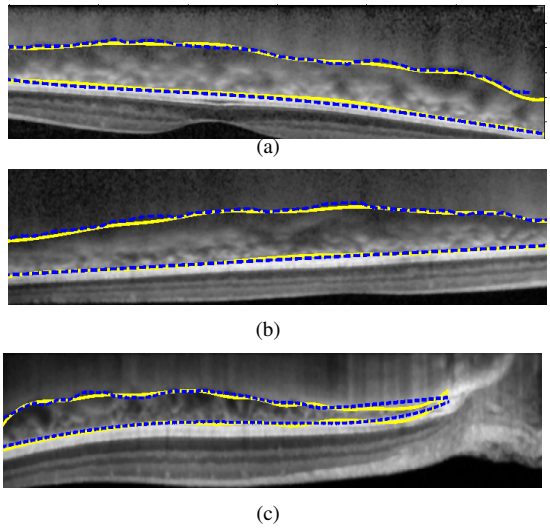

Fig. 7. Results of the choroid segmentation are indicated by the dash lines and ground truth labeled by the ophthalmologists is drawn in solid lines. (a) Dice coefficient= 98.93% (b) Dice coefficient = 95.35% (c) Dice coefficient=86.1%

References

[1] R. Margolis and R. F. Spaide, "A pilot study of enhanced depth imaging optical coherence tomography of the choroid in normal eyes." *Am J Ophthalmol*, vol. 147, no. 5, pp. 811–815, May 2009.

[2] H. A. Quigley, "What's the choroid got to do with angle closure?" *Archives of Ophthalmology*, vol. 127(5), pp. 693–4, May 2009.

[3] E. A. Maul, D. S. Friedman, D. S. Chang, M. V. Boland, P. Y. Ramulu, H. D. Jampel, and H. A. Quigley, "Choroidal thickness measured by spectral domain optical coherence tomography: factors affecting thickness in glaucoma patients." *Ophthalmology*, vol. 118, no. 8, pp. 1571–1579, Aug 2011.

[4] D. L. Nickla, C. Wildsoet, and J. Wallman, "The circadian rhythm in intraocular pressure and its relation to diurnal ocular growth changes in chicks." *Exp Eye Res*, vol. 66, no. 2, pp. 183–193, Feb 1998.

[5] D. Huang, E. A. Swanson, C. P. Lin, J. S. Schuman, W. G. Stinson, W. Chang, M. R. Hee, T. Flotte, K. Gregory, and C. A. Puliafito, "Optical coherence tomography." *Science*, vol. 254, no. 5035, pp. 1178–1181, Nov 1991.

[6] R. K. Wang, "Signal degradation by multiple scattering in optical coherence tomography of dense tissue: a monte carlo study towards optical clearing of biotissues." *Phys Med Biol*, vol. 47, no. 13, pp. 2281–2299, Jul 2002.

[7] R. F. Spaide, H. Koizumi, M. C. Pozzoni, and M. C. Pozonni, "Enhanced depth imaging spectral-domain optical coherence tomography." *Am J Ophthalmol*, vol. 146, no. 4, pp. 496–500, Oct 2008.

[8] S. E. Chung, S. W. Kang, J. H. Lee, and Y. T. Kim, "Choroidal thickness in polypoidal choroidal vasculopathy and exudative age-related macular degeneration." *Ophthalmology*, vol. 118, no. 5, pp. 840–845, May 2011.

[9] I. Maruko, T. Iida, Y. Sugano, A. Ojima, M. Ogasawara, and R. F. Spaide, "Subfoveal choroidal thickness after treatment of central serous chorioretinopathy." *Ophthalmology*, vol. 117, no. 9, pp. 1792–1799, Sep 2010.

[10] Y. Ikuno, K. Kawaguchi, T. Nouchi, and Y. Yasuno, "Choroidal thickness in healthy japanese subjects." *Invest Ophthalmol Vis Sci*, vol. 51, no. 4, pp. 2173–2176, Apr 2010.

[11] S. J. Chiu, X. T. Li, P. Nicholas, C. A. Toth, J. A. Izatt, and S. Farsiu, "Automatic segmentation of seven retinal layers in SDOCT images congruent with expert manual segmentation." *Opt Express*, vol. 18, no. 18, pp. 19 413–19 428, Aug 2010.

[12] Q. Yang, C. A. Reisman, Z. Wang, Y. Fukuma, M. Hangai, N. Yoshimura, A. Tomidokoro, M. Araie, A. S. Raza, D. C. Hood, and K. Chan, "Automated layer segmentation of macular OCT images using dual-scale gradient information." *Opt Express*, vol. 18, no. 20, pp. 21 293–21 307, Sep 2010.

[13] D. Koozekanani, K. Boyer, and C. Roberts, "Retinal thickness measurements from optical coherence tomgraphy using a markov boundary model," *IEEE Transactions on Medical Imaging*, vol. 20, pp. 906–916, 2001.

[14] V. Kaji, M. Esmaeelpour, B. Povaay, D. Marshall, P. L. Rosin, and W. Drexler, "Automated choroidal segmentation of 1060 nm OCT in healthy and pathologic eyes using a statistical mode," *Biomed. Opt. Express*, vol. 3, pp. 86–103, 2012.